Biosensors and Bioelectronics 94 (2017) 263–270

Contents lists available at ScienceDirect

Biosensors and Bioelectronics

journal homepage: www.elsevier.com/locate/bios

# Hybrid detection of target sequence DNA based on phosphorescence resonance energy transfer

Yanming Miao[1,*], Jinzhi Lv[1], Guiqin Yan[*]

*Shanxi Normal University, Linfen 041004, PR China*

ARTICLE INFO

*Keywords:*
Phosphorescence resonance energy transfer
Target sequence DNA
Quantum dots

ABSTRACT

The severe background fluorescence and scattering light of real biological samples or environmental samples largely reduce the sensitivity and accuracy of fluorescence resonance energy transfer sensors based on fluorescent quantum dots (QDs). To solve this problem, we designed a novel target sequence DNA biosensor based on phosphorescent resonance energy transfer (PRET). This sensor relied on Mn-doped ZnS (Mn-ZnS) room-temperature phosphorescence (RTP) QDs/poly-(diallyldimethylammonium chloride) (PDADMAC) nanocomposite ($QDs^+$) as the energy donor and the single-strand DNA-ROX as the energy receptor. Thereby, an RTP biosensor was built and used to quantitatively detect target sequence DNA. This biosensor had a detection limit of 0.16 nM and a linear range of 0.5–20 nM for target sequence DNA. The dependence on RTP of QDs effectively avoided the interference from background fluorescence and scattering light in biological samples. Moreover, this sensor did not need sample pretreatment. Thus, this sensor compared with FRET is more feasible for quantitative detection of target sequence DNA in biological samples. Interestingly, the $QDs^+$ nanocomposite prolonged the phosphorescence lifetime of Mn-ZnS QDs by 2.6 times to 4.94 ms, which was 5–6 magnitude-order larger than that of fluorescent QDs. Thus, this sensor largely improves the optical properties of QDs and permits chemical reactions at a long enough time scale.

## 1. Introduction

The resonance energy transfer theory was proposed early in 1948 (Förster, 1948). Resonance energy transfer is divided by the type of energy donor into fluorescence resonance energy transfer (FRET), whose donor is fluorescence materials (e.g. fluorescence proteins (Lewis and Daunert, 1999)), organic molecules (Milligan, 2004; Xia and Rao, 2009), inorganic fluorescence nano-materials (Su et al., 2014; Wang et al., 2010; Zhou et al., 2008; Peng et al., 2007; Zhang et al., 2005; Jiang et al., 2009), and bioluminescent resonance energy transfer (BRET), whose donor is luciferase or photoprotein (Xu et al., 1999; Oka et al., 2011). As excellent luminescent nanomaterials, quantum dots (QDs) are featured by narrow symmetrical emission spectrum, high luminescent efficiency, and photostability. QDs are very feasible for construction of FRET-based biosensors. QDs are widely used in small-molecule identification (Li et al., 2007), metal ion detection (Zhao et al., 2014), biological macromolecular detection (Haiyan et al., 2013; Wang et al., 2010; Su et al., 2014; Yang et al., 2016), cell imaging (Chen et al., 2012) and disease diagnosis (Tang et al., 2008). However, the severe background fluorescence and scattering light from real biological samples or environmental samples largely reduce the accuracy of fluorescent QD-based FRET sensors, which require complex sample pretreatment.

This defect is overcome by room-temperature phosphorescence (RTP) QDs. Since the triplet state of RTP allows for appropriately delaying the time for phosphorescence emission, the RTP QDs have much longer lifetime than fluorescent QDs. Thus, the phosphorescent detection avoids interference from background fluorescence and scattering light (Miao, 2015; Miao et al., 2015; He et al., 2009, 2008; Wu et al., 2010). Moreover, the less frequency of phosphorescence than fluorescence further improves the selectivity of phosphorescence sensors (Traviesa-Alvarez et al., 2007). Moreover, RTP spectrum is usually located at longer wavelengths and has larger Stokes shift, and thus does not overlap with the excitation spectrum, which avoids interference from the excitation light and modestly alleviates self-absorption. This is one cause for the high selectivity of RTP detection. Moreover, the QDs-based RTP detection does not require any deoxidant or inducer and avoids complex pretreatment (He et al., 2009; Wu et al., 2010; Sotelo-Gonzalez et al., 2012). Thus, RTP QDs are more feasible than fluorescent QDs for detection of target molecules in

* Corresponding authors.
*E-mail addresses:* mym8207@126.com (Y. Miao), gqyan2013@163.com (G. Yan).
[1] These authors contributed equally to this work and should be considered co-first authors.

http://dx.doi.org/10.1016/j.bios.2017.03.012
Received 20 December 2016; Received in revised form 26 February 2017; Accepted 6 March 2017
Available online 07 March 2017
0956-5663/ 

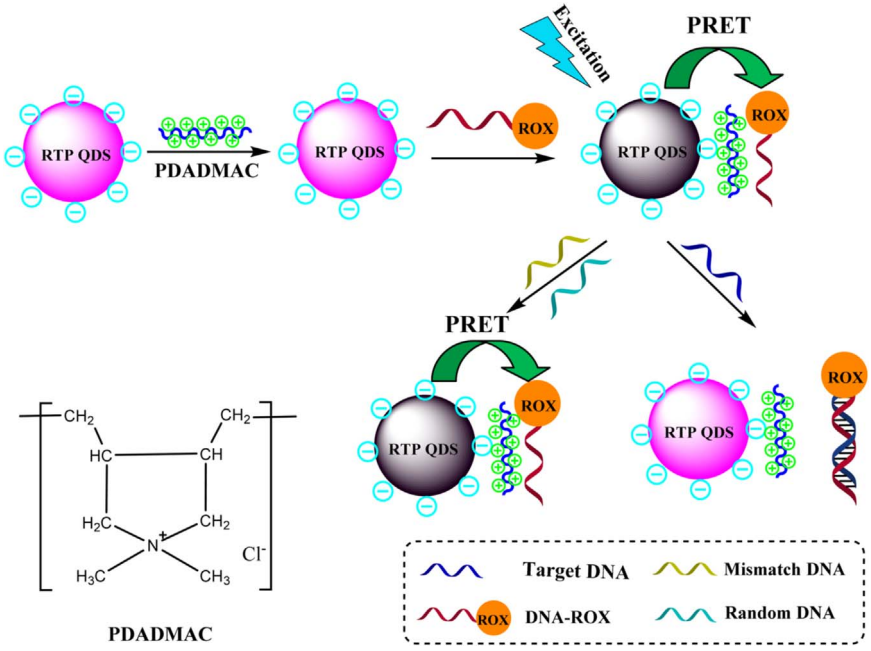


**Fig. 1.** Principle of DNA hybridization-detection system based on the RTP QDs/ROX-labeled DNA PRET.

complex biological samples, so RTP-QD-based sensors become a research hotspot (Wu et al., 2014a, 2014b, 2011, 2010; Miao et al., 2014a, 2014b, 2016, 2015; Miao, 2015; Gong and Fan, 2015; He and Yan, 2011; Zhang et al., 2013; Diaz-Diestra et al., 2017; Jin et al., 2016; Lv et al., 2017; Pacheco et al., 2017).

Based on the above reasons, RTP instead of fluorescence PRET biosensors or other sensors would largely expand the applications of resonance energy transfer. Due to the stability and sensitivity of resonance energy transfer sensors, we are able to produce PRET biosensors, biomolecular sensors and other types of sensors that are free from the interference of background fluorescence. However, there is rare research on PRET, and even less on PRET-based sensors.

The highlight of this study is that we developed an efficient PRET-based target sequence DNA sensor. This PRET sensor was built by using Mn-doped ZnS (Mn-ZnS) RTP QDs as the energy donor and DNA-ROX as the receptor. It is feasible for quantitative detection of target sequence DNA. The construction process is showed in Fig. 1. Specifically, Mn-ZnS QDs and poly-(diallyldimethylammonium chloride) (PDADMAC) electrostatically interacted to form Mn-ZnS QD/PDADMAC nanocomposite ($QDs^+$). As a result, the surfaces of Mn-ZnS QDs were positively charged, so after $QDs^+$ was added with the complementary signal-strand DNA-ROX (Rhodamine) of the target sequence, the negatively-charged single-strand DNA could electrostatically interact with $QDs^+$ to form $QDs^+$/DNA-ROX nanocomposite, so the RTP of $QDs^+$ was quenched by DNA-ROX via PRET. Then the target sequence DNA could complementarily match with DNA-ROX to form double-strand DNA, so the DNA-ROX competitively desorbed from the surfaces of $QDs^+$. As a result, the RTP of QDs+ was restored. Based on this principle, we built an RTP sensor for quantitative detection of target sequence DNA. The dependence on the RTP of QDs effectively avoids interferences from background fluorescence and scattering light of biological samples. Moreover, this sensor does not need sample pretreatment, so it is especially suitable for quantitative detection of target sequence DNA in biological samples.

## 2. Experimental

### 2.1. Materials and chemicals

MPA (J & K Scientific, Beijing, China), $Zn(Ac)_2{\cdot}2H_2O$, $Mn(Ac)_2{\cdot}4H_2O$, and $Na_2S{\cdot}9H_2O$ (Tianjing Kermel Chemical Reagent Co., China) were used to prepare Mn-doped ZnS QDs. Ultrapure water (18.2 MΩ cm) was obtained from a Water Pro water purification system (Labconco Corporation, Kansas City, MO). PDADMAC was provided by (Aladdin, Shanghai, China). DNA sequences were synthesized by Sangon Biotech (Shanghai).

The sequences involved were:

Target DNA (complementary DNA): 5′-CAT CGT TGA AGA TGC CTC TGC CG-3′.

Probe DNA-ROX: 5′– CGG CAG AGG CAT CTT CAA CGA TG -ROX-3′.

Single-base mismatch DNA: 5′-CAT CGT TGA AGA TCC CTC TGC CG-3′.

Random DNA: 5′-TCA TTC CAG CTC GTA ACG CTA TAG ATA-3′.

### 2.2. Apparatuses

Phosphorescence was measured by a Cary Eclipse fluorescence spectrophotometer (Varian American Pty Ltd., America), equipped with a plotter unit and a quartz cell (1×1 $cm^2$). The morphology and microstructure of QDs and QDs-DNA were characterized by a JEM-2100 transmission electron microscope (TEM, Japan). Resonance light scattering (RLS) spectra were recorded in the same spectrofluorometer by simultaneously scanning the excitation and emission monochromators (Δλ=0) from 200 to 700 nm. Other apparatuses included a pH meter (Jinpeng Analytical Instruments Co. Ltd, China) and a Shimadzu UV-29100 ultraviolet/visible spectrophotometer.

### 2.3. Synthesis of Mn-doped ZnS QDs

MPA-capped Mn-ZnS QDs were prepared as described before (Miao et al., 2016; Wu et al., 2010; Zhuang et al., 2003; He et al., 2009). First,

$Zn(Ac)_2$ (5 mL, 0.1 mol $L^{-1}$), $Mn(Ac)_2$ (2 mL, 0.01 mol $L^{-1}$) and MPA (50 mL, 0.04 mol $L^{-1}$) were added into a 100-mL three-necked bottle. The mixture was adjusted to pH 11 by adding a 1 mol $L^{-1}$ NaOH solution, then magnetically stirred at room temperature and ventilated with argon gas for 30 min. Then under air isolation, 5 mL of 0.1 mol $L^{-1}$ $Na_2S$ was injected in, followed by argon gas ventilation for 20 min. After atmospheric ageing for 2 h, the resulting solution was maintained at 50 °C, thus forming MPA-capped Mn-ZnS QDs. A same volume of ethanol was added to precipitate the QDs. After centrifugation, washing with ethanol, and vacuum oven drying for 24 h, finally powder MPA-capped Mn-ZnS QDs were formed.

### 2.4. Synthesis of $QDs^+$

Then the Mn-ZnS QDs (5 mg) were dissolved in ultrapure water, followed by addition of PDADMAC (100 μL, 35 wt%). The mixture was diluted to 10 mL, shaken evenly, and put still for 10 min. Then after addition of anhydrous ethanol (10 mL), the resulting solution was shaken evenly and centrifuged. The resulting supernatants were discarded. Each experiment was conducted in triplicate. Finally, the resulting solution was diluted in a phosphate buffer solution (PBS; 5 mL, 20 mM, pH 7.4). Then a 1 mg/mL (calculated as per the Mn-ZnS QDs) Mn-ZnS QDs/PDADMAC ($QDs^+$) nanocomposite solution was prepared.

### 2.5. General experimental procedure

To study the effects of DNA-ROX on the RTP intensity of $QDs^+$, we first prepared a 1.0 μM DNA-ROX aqueous solution. Then the PBS (pH 7.4, 20 mM) was added with 50 μL of the $QDs^+$ solution. Then a series of DNA-ROX test solutions at different concentrations were prepared by adding different volumes of DNA-ROX solution. All solutions were diluted to 5 mL, shaken evenly and after 30 min, they were sent to RTP detection at the excitation wavelength 295 nm. For detection of target DNA, first the target DNA was dissolved in water to form a 1.0 μM solution. Then the PBS (20 mM, pH 7.4) was added with $QDs^+$(50 μL), DNA-ROX (200 μL) and the target DNA solution (0–80 nM). The resulting solutions were diluted to 5 mL, shaken evenly and after 30 min, were sent to RTP detection.

### 2.6. Molecular dynamics simulation of DNA-ROX and target sequence DNA

(1) DNA system construction

The sense primer and anti-sense primer of two standard B-DNA chains were constructed on Discovery Studio 3.5 as follows: 5′- CGG CAG AGG CAT CTT CAA CGA TG −3′, and 5′- CAT CGT TGA AGA TGC CTC TGC CG-3′ [DNA(WT)]; 5′- CGG CAG AGG CAT CTT CAA CGA TG −3′, and 5′-CAT CGT TGA AGA TCC CTC TGC CG-3′ [DNA(MT)].

(2) Simulation conditions

Molecular dynamics simulation of two DNA systems [DNA(WT), DNA(MT)] were conducted on Gromacs 4.6.7. DNA was put into a periodically tetrahedron box, under an Amber99sb force field. The smallest space from the solute to the box edges was 1.2 nm. Long-course electrostatic interaction was based on PME. After every 10 steps of simulation, the non-bonded interaction pair table was updated one time. The grid width was 0.12 nm. The L-J interactional sectional distance was 0.9 nm. Water as single-dot charge model was used. The unreasonable energy barrier was eliminated by 1000-step energy optimization via the steepest descent method. NaCl solution was added to make the simulation system neutral. From the initial conformations, solute atoms were restrained in the 100 ps restrained dynamics simulation. The temperature was raised stepwise to 300 K. Thus, the two systems were both maintained at 300 K and $10^5$ Pa. At the step of 2 fs, the two systems were separately simulated via NPT for 100 ps.

(3) Steered molecular dynamics simulation

With steered molecular dynamics, one DNA strand was imposed by a constant speed force to pull away the double strands. At the steering speed of 0.04 nm/ps, the centroid distance increased from 0.5 to 5.0 nm, forming 10 different conformations. After that, from the above initial structures of these systems, free dynamics simulation at 300 K was conducted for 10 ns. The potential of mean force (PMF) was obtained via weighted orthogonal analysis, and the free energy of dissociation was determined.

### 2.7. Sample pretreatment

Serum and urine samples were collected from healthy volunteer. Samples were subjected to a 100-fold dilution before analysis and no other pretreatments were used.

### 2.8. Sample detection

Each time, PBS (0.5 mL, 0.2 M), DNA-ROX (200 μL, 1.0 μM), $QDs^+$(50 μL, 1 mg/mL), serum or urine (0.05 mL) were successively added into a 5 mL colorimetric tube. The resulting solution was added with different volumes of the target DNA solutions, and diluted with ultrapure water to 5 mL. The target DNA solutions were spiked to 5.0 and 10.0 nM, shaken evenly, and placed still for 30 min, followed by RTP detection at 295 nm. All experiments were conducted in triplicate. The serum and urine samples were diluted 100 times, without any other pretreatment.

## 3. Results and analysis

### 3.1. Characteristics of Mn-$ZnS^+$ QDs

The shape and size of MPA-capped Mn-$ZnS^+$ QDs were characterized by TEM, which showed the diameter was about 3.5 nm (Fig. S1A). The QDs had the largest excitation peak at 295 nm (curve a in Fig. S1B) and the largest emission peak at 590 nm (curve b). The RTP is attributed to the transition of $Mn^{2+4}T_1$-$^6A_1$ (Yildiz et al., 2006). After the excitation, the excitation light was absorbed by the ZnS matrix, which thus stimulated its electrons. The holes as-formed captured $Mn^{2+}$, while the electrons and holes separately formed composites with $Mn^{2+}$, which led to the excitation of $Mn^{2+}$ and energy release in the of RTP (about 590 nm) (Thakar et al., 2007).

The $pK_{COOH}$ of MPA was 4.3 on surfaces of QDs, so the QDs were negatively- charged on surfaces in the pH 7.4 PBS, while the PDADMAC was strongly positively-charged. As a result, the two substances aggregated via electrostatic interaction to form positively-charged $QDs^+$. After the formation of $QDs^+$, the excitation of QDs and the shape of emission spectrum were basically unchanged, but the RTP intensity was slightly enhanced (curves c, d, Fig. S1B). The possible reason is that PDADMAC can simultaneously bind several QDs, which shortened the distances between some Mn-ZnS QDs. The TEM images (Fig. S1C) also show the obvious QD aggregation. Since the surface defects atop QDs caused by electrons- holes resulted in the formation of local electric field (Norris et al., 1994; Klimov, 2000), the reduced between-QD distance would enhance the local electric field around the QDs and stimulate the QDs to generate more-effective excitation (Kulakovich et al., 2002; Anger et al., 2006). As a result, more energy transferred from the surface holes of Mn-ZnS QDs to $Mn^{2+}$, which thus significantly enhanced the RTP intensity of Mn-ZnS QDs (He et al., 2009; Hou et al., 2008). On the contrary, $Mn^{2+}$ was located in ZnS crystal lattices, whose luminescence center was basically not impacted, so the relative positions of the excitation and emission spectra were generally unchanged (Huynh et al., 2002).

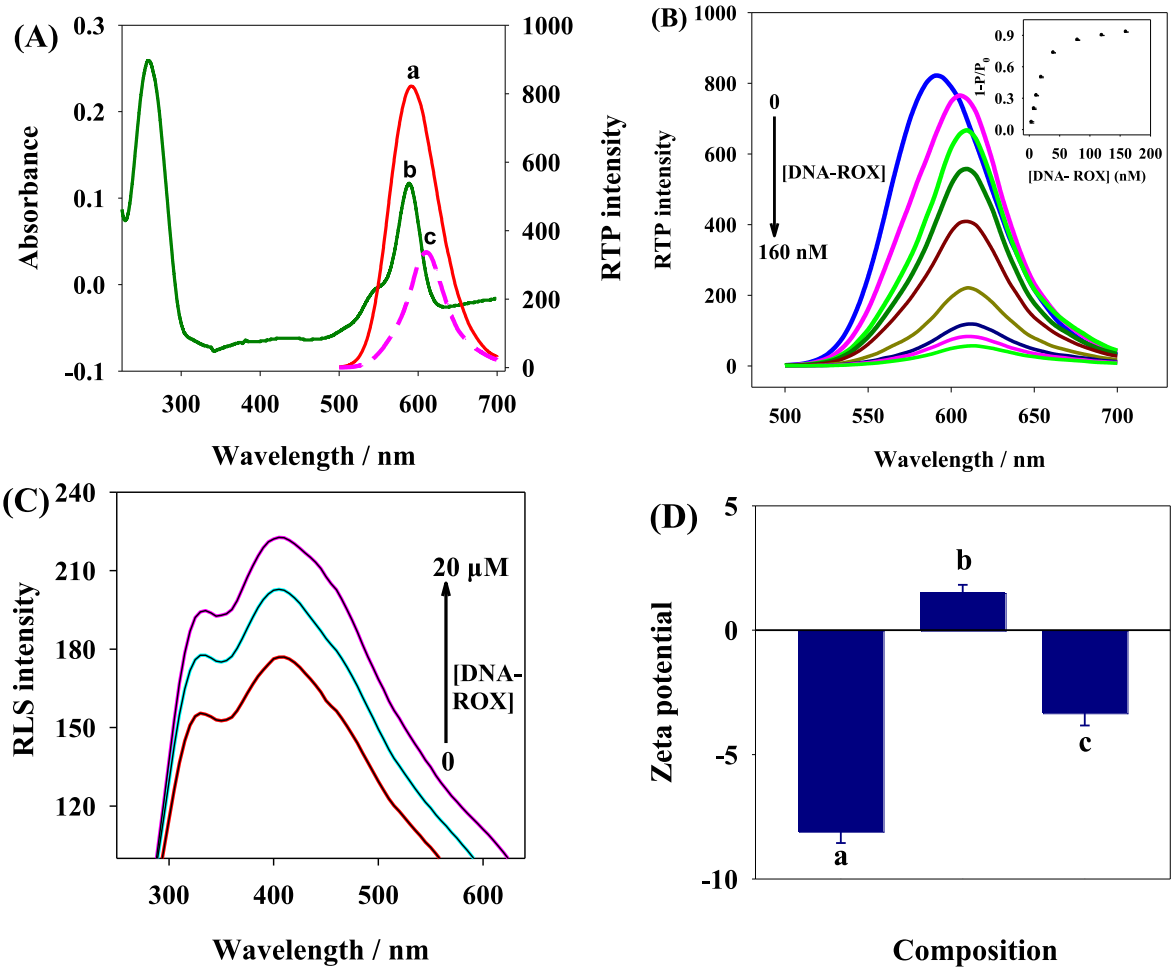


**Fig. 2.** (A) Spectra of (a) RTP emission of Mn-ZnS QDs excited at 295 nm, (b) absorption of DNA-ROX, and (c) emission of $QDs^+$/DNA-ROX excited at 295 nm; (B) DNA-ROX concentration-dependent RTP emission of the $QDs^+$(10 mg $L^{-1}$); The inset shows the change of the RTP intensity with the increase of the concentration of DNA-ROX; (C) RLS spectra of the $QDs^+$(10 mg $L^{-1}$) in the presence of various concentrations of DNA-ROX; (D) The zeta-potential histogram of Mn-ZnS QDs (histogram a), $QDs^+$(histogram b) and $QDs^+$/DNA-ROX (histogram c). All spectra were recorded in PBS buffer (20 mM, pH 7.4).

### 3.2. Interaction between $QDs^+$ and DNA-ROX

As for DNA-ROX, the presence of ROX accounted for the large ultraviolet absorption at 585 nm (Fig. 2A), while the emission spectrum of $QDs^+$(curve a) is partially overlapped with the absorption spectrum of DNA-ROX (curve b). Thus, after the electrostatic interaction between DNA-ROX and $QDs^+$, the DNA-ROX could absorb a part of the phosphorescence emitted by $QDs^+$. In other words, PRET occurred between $QDs^+$(the energy donor) and DNA-ROX (the receptor), leading to the energy transfer from $QDs^+$ to DNA-ROX, which quenched the RTP of $QDs^+$(curve c).

Fig. 2B shows the variation of RTP intensity of $QDs^+$ after the addition of DNA-ROX. The RTP intensity of $QDs^+$ is gradually weakened as the concentration of DNA-ROX rises, accompanied by red shift. This is because the phosphorescence emission spectrum of $QDs^+$ partially overlaps with the absorption spectrum of DNA-ROX. When the concentration of DNA-ROX is above 40 nM, the change in the RTP intensity of $QDs^+$ gradually stabilizes (inset in Fig. 2B).

If two substances can aggregate through interaction and produce scattering particles, they can generate very remarkable RLS. Fig. 2C shows the variation of RLS signals of $QDs^+$ after the addition of DNA-ROX. The RLS intensity was gradually enhanced after DNA-ROX was slowly added into the $QDs^+$ solutions, indicating $QDs^+$ and DNA-ROX had formed larger nanocomposite particles. This is because PDADMAC was capped atop the Mn-ZnS QDs, making the QDs positively charged ($QDs^+$), while DNA-ROX was negatively-charged in weak alkaline solution (pH 7.4) due to the presence of DNA strands. Thus, $QDs^+$ and DNA-ROX could electrostatically interact to form larger $QDs^+$/DNA-ROX nanocomposites.

Fig. 2D shows the Zata potentials of Mn-ZnS QDs (histogram a), $QDs^+$(histogram b) and QDs+/DNA-ROX (histogram c). Clearly, the potential of Mn-ZnS QDs is $-8.08 \pm 0.478$ (histogram a), but it increases to $1.52 \pm 0.307$ after capping with PDADMAC (histogram b). The QDs became positively charged after the addition of DNA-ROX. This is because the DNA-ROX adhered via electrostatic attraction to the surfaces of $QDs^+$, but due to the negative charge of DNA-ROX, the potential became negative again ($-3.32 \pm 0.513$, histogram c).

The above results indicate that the DNA-ROX and $QDs^+$ electrostatically interacted to form $QDs^+$/DNA-ROX nanocomposite, and the DNA-ROX quenched, through PRET, the RTP of $QDs^+$.

### 3.3. Mechanism how DNA-ROX quenches $QDs^+$

Phosphorescent quenching is divided into dynamic quenching and static quenching. Dynamic quenching is an interaction between the excited state molecules of quenchers and phosphorescent substances, thus reducing the phosphorescent intensity. This process obeys the Stern-Volmer equation (Eq. 1). Static quenching is a coordination at the ground state between the quencher and the phosphorescent substance, and the resulting nonluminous coordination compounds would reduce the phosphorescent intensity. This process obeys the Lineweaver- Burk double-reciprocal curve (Eq. (2)) (Kenneth et al.,

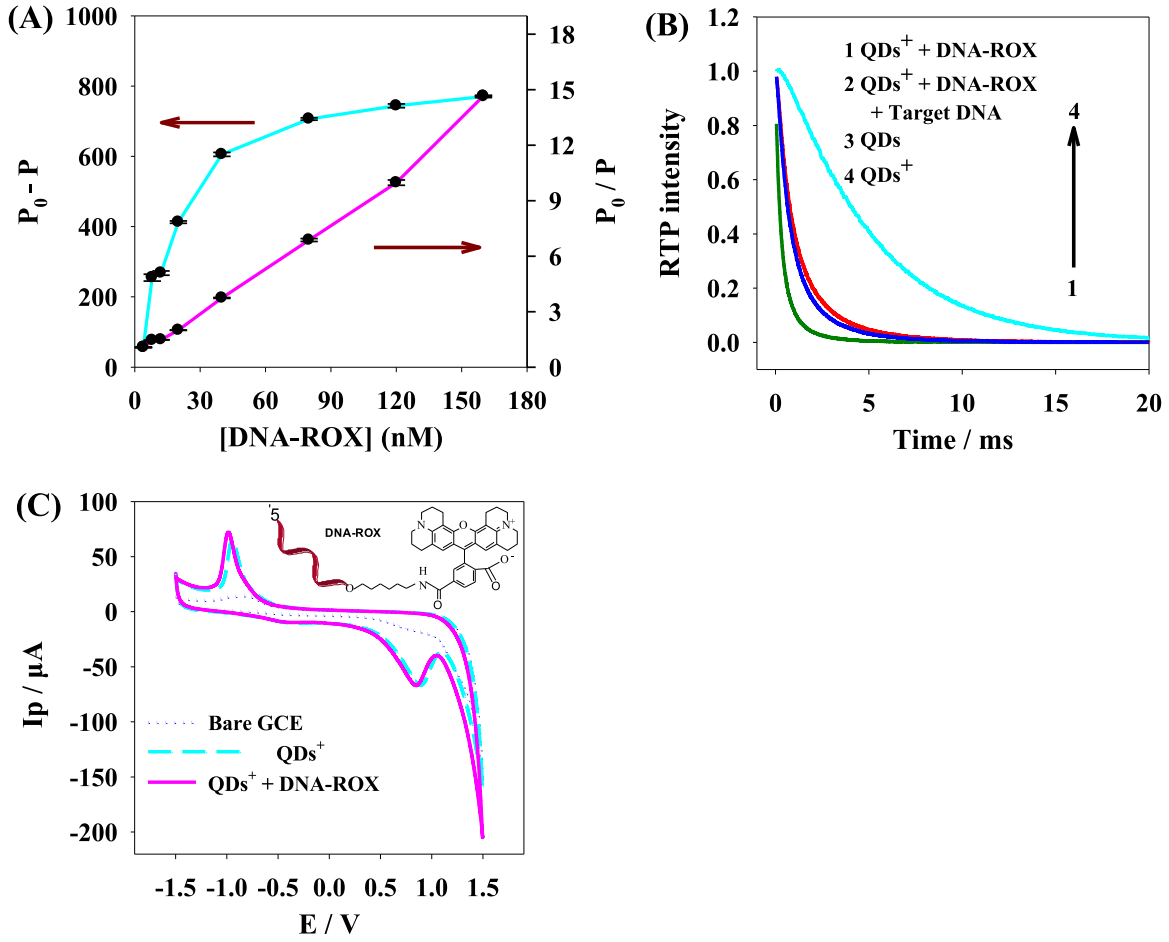


**Fig. 3.** (A) The Lineweaver-Burk plot and Stem-Volmer plot of phosphorescence quenching of $QDs^+$;(B)The decay curves of QDs, $QDs^+$, $QDs^+$+ DNA-ROX and $QDs^+$/DNA-ROX+Target DNA; (C)The cyclic voltammograms of bare glassy carbon electrode (GCE) (blue line), GCE modified with Mn-ZnS $QDs^+$(cyan line), and GCE modified $QDs^+$/DNA-ROX mixture(pink line) with a scan rate of 100 $mV/s^{-1}$. (For interpretation of the references to color in this figure legend, the reader is referred to the web version of this article.).

1987; Lakowicz and Weber, 1973; He et al., 2008):

$$P_0/P = 1 + K_{SV}C_q \quad (1)$$

$$1/(P_0-P)=1/P_0+K_{LB}/(P_0C_q) \quad (2)$$

where $P_O$ is the phosphorescent intensity of the phosphor; $P$ is the phosphorescent intensity after addition of a quencher; $C_q$ is the concentration of the quencher. $K_{SV}$ is a Stern-Volmer constant that reflects the phosphorescent molecules and the phosphorescent quencher would spread and collide until they reach a balanced dose-effect relationship. $K_{LB}$ is a static quenching binding constant (Jones et al., 2001; Murphy et al., 2004; Baptista and Indig, 1998; Lakowitz, 1999). Fig. 3A shows the Stern-Volmer equation and Lineweaver-Burk curve fitted from experimental data. Results show the concentration relationship between $P_O/P$ and DNA-ROX obeys the Stern-Volmer equation. The course of DNA-ROX quenching $QDs^+$ is a dynamic process.

The interaction between DNA-ROX and $QDs^+$ was further investigated by studying the variation of phosphorescence lifetime. Fig. 3B shows the phosphorescence lifetime of QDs, $QDs^+$, $QDs^+$/DNA-ROX, and $QDs^+$/DNA-ROX/ target DNA. Results show that after capping by PDADMAC, the phosphorescence lifetime of QDs was prolonged by 2.6 times from 1.86 to 4.94 ms. After $QDs^+$ were added to DNA-ROX, the total phosphorescence lifetime was shortened to 0.77 ms, indicating the occurrence of dynamic quenching between $QDs^+$ and DNA-ROX. After $QDs^+$/DNA-ROX was added with the target DNA, the total phosphorescence lifetime was restored, further indicating the occurrence of dynamic quenching between $QDs^+$ and DNA-ROX.

To validate that the interaction between QDs+ and DNA-ROX was PRET but not electron transfer, we studied the electrochemical properties of this interaction. As showed in Fig. 3C, the oxidation reducing peaks between $QDs^+$ and $QDs^+$/DNA-ROX are basically overlapped, so we think only PRET, but no electron transfer, has occurred between $QDs^+$ and DNA-ROX. The possible reason is that the electron transfer depends more strictly on the donor-receptor distance, which is much shorter than that required by PRET (Newton, 1991). Though the strong negative charge at the DNA end of DNA-ROX facilitated the binding between $QDs^+$ and DNA-ROX, accompanied by PRET, the positive charge of $N^+$ at the ROX end mutually repelled with $QDs^+$, which prolonged the distance between $QDs^+$ and ROX. As a result, the distance between the ROX end and $QDs^+$ was not long enough to support the electron transfer, but allowed PRET.

To study the quenching rate of free PDADMAC, we investigated how the addition of PDADMAC affected the QDs and DNA-ROX system. Results show (Fig. S2) when the concentration of PDADMAC rises from $7\times10^{-6}$ wt% to $2.1\times10^{-5}$ wt%, the systematic phosphorescence intensity gradually declines, but it increases again beyond the concentration of $6.3\times10^{-5}$ wt%. This is because the low-concentration PDADMAC could bind QDs and DNA-ROX together, so DNA-ROX quenched the RTP of QDs. However, at very high concentrations, a part of free PDADMAC first binds with DNA-ROX, besides the binding with QDs. This reduced the binding between DNA-ROX and QDs, so the presence of high-concentration PDADMAC led to the rise of RTP of QDs. DNA-ROX is the first to bind with the free PDADMAC because in solution, the polymer chains have a conformation of a flexible random coil, which facilitates their interaction with ssDNA through electrostatic and hydrophobic interactions (Peng et al., 2007).

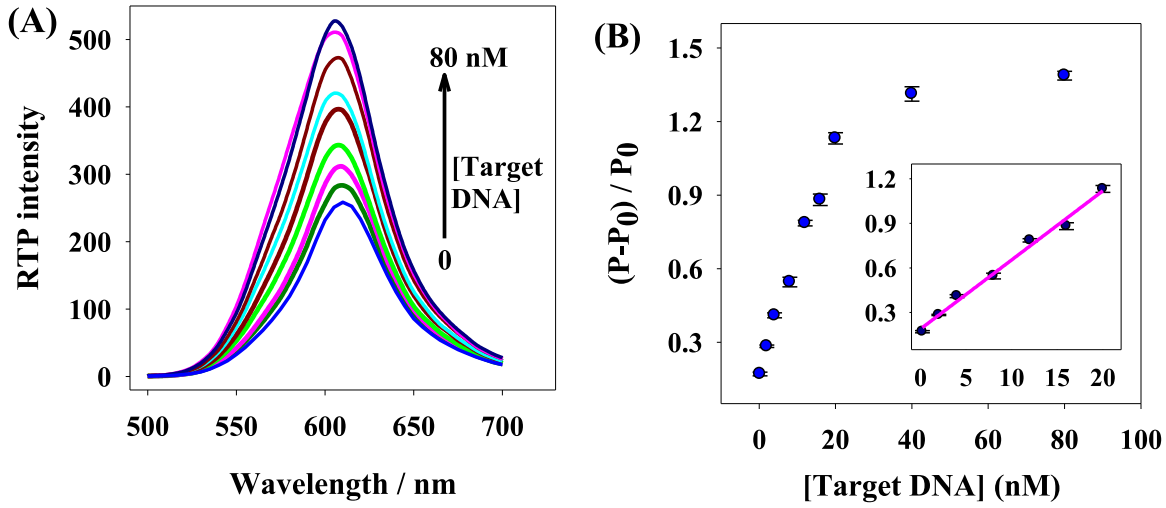


**Fig. 4.** (A) Target sequence DNA concentration-dependent RTP emission of the $QDs^+$ nanohybrids; (B) Plots of RTP as a function of target sequence DNA concentration show linear range. Buffer, 20 mM PBS (pH 7.4); $QDs^+$, 10 mg $L^{-1}$.

These results suggest that the interaction between DNA-ROX and $QDs^+$ is a dynamic quenching process, and largely reduces the concentration of free PDADMAC.

### 3.4. $QDs^+$/ DNA-ROX nanocomposite used to detect target DNA

As showed in Fig. 4A, with the rise of target DNA concentration, the RTP intensity of $QDs^+$/DNA-ROX nanocomposite is regularly restored, indicating this nanocomposite can be used as an RTP probe to detect the target DNA. According to these results, we designed a method based on the $QDs^+$/DNA-ROX nanocomposite for detection of RTP target sequence DNA. At pH 7.4, the change of RTP intensity of the $QDs^+$/DNA-ROX nanocomposite ($(P-P_0)/P_0$) is linearly correlated with the concentration of target sequence DNA within a certain range (Fig. 4B).

This RTP sensor in detection of target sequence DNA had a linear range of 0.5–20 nM and a detection limit of (3σ) 0.16 nM. The precision from 11 parallel measurements of 5 nM target sequence DNA was 2.6%. This detection limit is lower than the non-specific RTP DNA detection method and the specific fluorescent DNA detection method (Table 1) (He et al., 2009; Miao et al., 2014a, 2014b, 2015; Bi and Yu, 2015; Ye et al., 2016; Wang et al., 2010; Zhou et al., 2008). The benefit of this method is that it utilizes PRET to identify and detect specific sequence DNA by taking advantage of RTP, so it is not interfered by the background fluorescence or scattering light of biological fluids, and it does not need complex sample pretreatment. This method is feasible for detection of viral DNA, transgene promoter characteristic DNA, and biomedicine specific DNA.

To prove that the quenching of RTP was not induced by the direct action of target sequence DNA on $QDs^+$, we added 20 nM target sequence DNA into $QDs^+$ solutions. Results show the target sequence DNA did not significantly affect the RTP intensity of $QDs^+$(Fig. S3).

### 3.5. Molecular dynamics simulation and selectivity of $QDs^+$/DNA-ROX over target sequence DNA

By analyzing how $QDs^+$/DNA-ROX nanocomposite could identify complementary DNA, single-base-mismatched DNA, and random DNA (Fig. 5A), we found the new RTP biosensor was highly selective to the target sequence DNA and can selectively identify and detect target sequence DNA.

To further elucidate the mechanism about its selectivity, we designed molecular dynamics simulations between DNA-ROX (DNA in DNA-ROX was involved in the computation) and complementary DNA or single-base-mismatched DNA (Fig. 5B). Results show that the binding with complementary DNA compared with single-base- mismatched DNA was less stable. When the centroid of two strands was less than 1.0 nm, with the prolonging of tensile time, the free energy of dissociation gradually rose. At the same steering distance, the double-stranded DNA formed from DNA-ROX and single-base-mismatched DNA (marked as DNA(WT)) needed less free energy than the double-strand formed from DNA-ROX and complementary DNA (marked as DNA(MT)), indicating DNA(MT) is less stable and its dissociation consumes less free energy. When the steering distance was larger than 1.0 nm, the steering force gradually stabilized. When DNA(MT) was larger than 0.9 nm, the dissociation free energy first rose largely and then dropped to the level of DNA(WT), suggesting that the steering distance of DNA double strands that was larger than the threshold could destroy the hydrogen bond interaction.

**Table 1**
Comparison of biosensor performances for DNA detection with different optical schemes.

| Method | Linear range | Detection limit | Reference |
|---|---|---|---|
| RTP of Mn-doped ZnS QDs | 0.1–14 mg $L^{-1}$. | 0.039 mg $L^{-1}$ | (Miao et al., 2014a) |
| RTP of Mn-doped ZnS QDs | 0.033–20 mg $L^{-1}$. | 0.033 mg $L^{-1}$ | (Miao et al., 2015) |
| RTP of Mn-doped ZnS QDs | 0.125–10 μM | 54.9 nM | (He et al., 2009) |
| RTP of Mn-doped ZnS QDs | 0.2–20 mg $L^{-1}$ | 0.045 mg $L^{-1}$ | |
| Fluorescence of the AgNCs | 1–50 nM | 0.4 nM | (Ye et al., 2016) |
| Fluorescence of the QDs | 0–50 nM | 4.0 nM | (Wang et al., 2010) |
| Fluorescence of the QDs | 0–200 nM | 1.0 nM | (Zhou et al., 2008) |
| RTP of Mn-doped ZnS QDs | 0.5–20 nM | 0.16 nM ( 0.001 mg $L^{-1}$ ) | This work |

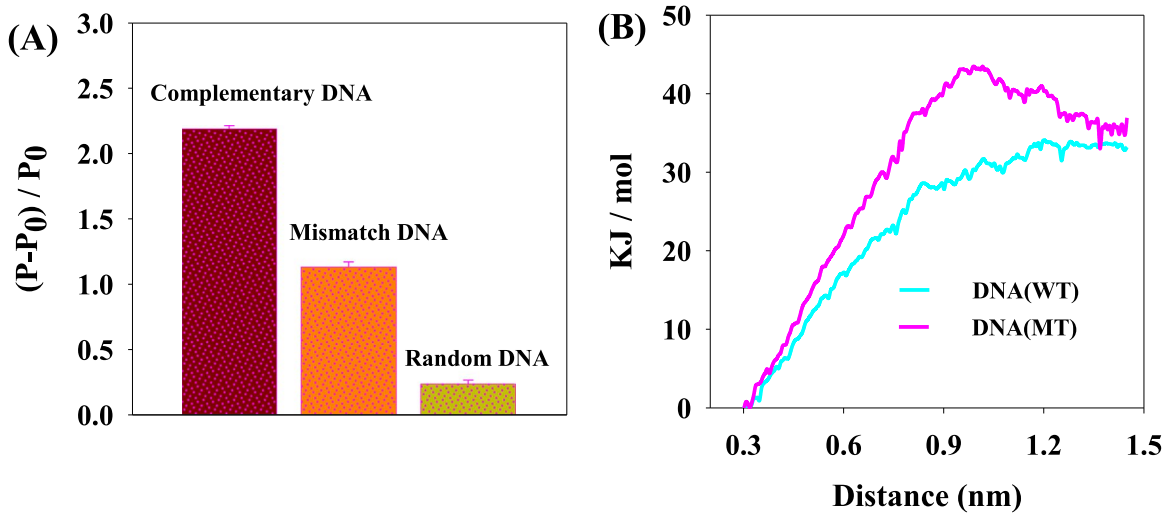


**Fig. 5.** (A) Detection characteristics of QDs$^{+}$/DNA-ROX nanocomposites over complementary DNA, single-base-mismatched DNA, and random DNA; (B) Variation of dissociation free energy along with the between-strand distance, DNA(WT) is normal DNA1, DNA(MT) is mutant DNA2.

### *3.6. Sample analysis*

Fig. S4 indicates that the human urine and serum do not produce background phosphorescence (curve 1 and curve 2), but generate background fluorescence (curve 3 and curve 4). The reason is that the human fluids contain many proteins and biomolecules that can produce autofluorescence, but rarely generate autophosphorescence. Therefore, this sensor is basically not interfered with the autofluorescence of biofluids, and is very suitable for DNA detection in biofluids.

To validate whether the QDs$^{+}$/DNA-ROX nanocomposite could detect and identify the target sequence DNA in real biological samples, we designed the spiked recovery experiments for target sequence DNA in serum and urine samples. The concentrations of target DNA were 5 and 10 nM, respectively, and the spiked recovery rates of urine and serum samples were 95–103% (Table S1).

### *3.7. Selectivity of QDs+/DNA-ROX DNA RTP probe*

The common metal ions and biomolecules in biological fluids were used to study their interferences on the QDs$^{+}$/DNA-ROX probe. With the presence of 10 nM target DNA, we found $2.0\times10^{5}$-fold $K^{+}$, $5.0\times10^{5}$-fold $Na^{+}$, $2.0\times10^{4}$-fold $Ca^{2+}$, $1.0\times10^{4}$-fold $Mg^{2+}$, $2.0\times10^{4}$-fold glucose, $5.0\times10^{3}$-fold L-cysteine, $1.0\times10^{4}$-fold L-histidine, or $1.0\times10^{4}$-fold glycin did not significantly affect the RTP intensity of this DNA system (Table S2).

## 4. Conclusions

A QDs$^{+}$ nanocomposite was prepared from Mn-doped ZnS RTP QDs and PDADMAC. The phosphorescence lifetime of QDs was prolonged by 2.6 times. With QDs as the energy donor and DNA-ROX as the receptor, an efficient PRET-based DNA sequence sensor was built and used to quantitatively detect target DNA sequences. This biosensor had a detection limit of 0.16 nM and a linear range of 0.5–20 nM for target DNA sequence. The dependence on the RTP of QDs effectively avoids interferences from background fluorescence and scattering light of biological samples. Moreover, this sensor does not need sample pretreatment, so it is especially suitable for quantitative detection of target sequence DNA in biological samples.

## Acknowledgments

This work was supported by the funds of the Natural Science Foundation for Young Scientists of Shanxi Province (201601D021109) and Construction Program of Chemical Advantage and Key discipline of Shanxi Province of China (Grant 912019).

## Appendix A. Supporting information

Supplementary data associated with this article can be found in the online version at doi:10.1016/j.bios.2017.03.012.

## References

Anger, P., Bharadwaj, P., Novotny, L., 2006. Phys. Rev. Lett. 96, 113002.
Baptista, M.S., Indig, G.L., 1998. J. Phys. Chem. B 102, 4678–4688.
Bi, L., Yu, Y.-H., 2015. Spectrochim. Acta A: Mol. Biomol. Spectrosc. 140, 479–483.
Chen, L., Zhang, X., Zhou, G., Xiang, X., Ji, X., Zheng, Z., He, Z., Wang, H., 2012. Anal. Chem. 84, 3200–3207.
Diaz-Diestra, D., Thapa, B., Beltran-Huarac, J., Weiner, B.R., Morell, G., 2017. Biosens. Bioelectron. 87, 693–700.
Förster, T., 1948. Ann. Phys.-Berl. 437, 55–75.
Gong, Y., Fan, Z., 2015. Biosens. Bioelectron. 66, 533–538.
Haiyan, C., Bowen, L., Chuan, W., Xin, Z., Zhengqi, C., Xi, D., Rui, Z., Yueqing, G., 2013. Nanotechnology 24, 055704.
He, Y., Wang, H.-F., Yan, X.-P., 2008. Anal. Chem. 80, 3832–3837.
He, Y., Wang, H.-F., Yan, X.-P., 2009. Chem.-A Eur. J. 15, 5436–5440.
He, Y., Yan, X., 2011. Sci. China Chem. 54, 1254.
Hou, Y., Ye, J., Gui, Z., Zhang, G., 2008. Langmuir 24, 9682–9685.
Huynh, W.U., Dittmer, J.J., Alivisatos, A.P., 2002. Science 295, 2425–2427.
Jiang, G., Susha, A.S., Lutich, A.A., Stefani, F.D., Feldmann, J., Rogach, A.L., 2009. ACS Nano 3, 4127–4131.
Jones, R.M., Bergstedt, T.S., McBranch, D.W., Whitten, D.G., 2001. J. Am. Chem. Soc. 123, 6726–6727.
Jin, Q., Li, Y., Huo, J., Zhao, X., 2016. Sens. Actuators B: Chem. 227, 108–116.
Kenneth, S., Hugo, S., Peter, S., 1987. Photochem. Photobiol. 46, 427–440.
Klimov, V.I., 2000. J. Phys. Chem. B 104, 6112–6123.
Kulakovich, O., Strekal, N., Yaroshevich, A., Maskevich, S., Gaponenko, S., Nabiev, I., Woggon, U., Artemyev, M., 2002. Nano Lett. 2, 1449–1452.
Lakowicz, J.R., Weber, G., 1973. Biochemistry-US 12, 4161–4170.
Lakowitz, J.R., 1999.
Lewis, J.C., Daunert, S., 1999. Anal. Chem. 71, 4321–4327.
Li, H., Zhang, Y., Wang, X., Xiong, D., Bai, Y., 2007. Mater. Lett. 61, 1474–1477.
Lv, J., Miao, Y., Yang, J., Qin, J., Li, D., Yan, G., 2017. Biosens. Bioelectron. 91, 560–565.
Miao, Y., 2015. RSC Adv. 5, 76804–76812.
Miao, Y., Li, Y., Zhang, Z., Yan, G., Bi, Y., 2015. Anal. Biochem. 475, 32–39.
Miao, Y., Yang, M., Yan, G., 2016. RSC Adv. 6, 8588–8593.
Miao, Y., Zhang, Z., Gong, Y., Yan, G., 2014a. Biosens. Bioelectron. 59, 300–306.
Miao, Y., Zhang, Z., Gong, Y., Zhang, Q., Yan, G., 2014b. Biosens. Bioelectron. 52, 271–276.
Milligan, G., 2004. Eur. J. Pharm. Sci. 21, 397–405.
Murphy, C.B., Zhang, Y., Troxler, T., Ferry, V., Martin, J.J., Jones, W.E., 2004. J. Phys. Chem. B 108, 1537–1543.
Newton, M., D., 1991. Chem. Rev. 91, 767–792.
Norris, D., Sacra, A., Murray, C., Bawendi, M., 1994. Phys. Rev. Lett. 72, 2612–2615.
Oka, T., Takagi, H., Tohya, Y., Murakami, K., Takeda, N., Wakita, T., Katayama, K., 2011. Antivir. Res. 90, 9–16.
Pacheco, M.E., Castells, C.B., Bruzzone, L., 2017. Sens. Actuators B: Chem. 238,

660–666.
Peng, H., Zhang, L., Kjällman, T.H.M., Soeller, C., 2007. J. Am. Chem. Soc. 129, 3048–3049.
Sotelo-Gonzalez, E., Fernandez-Argüelles, M.T., Costa-Fernandez, J.M., Sanz-Medel, A., 2012. Anal. Chim. Acta 712, 120–126.
Su, S., Fan, J., Xue, B., Yuwen, L., Liu, X., Pan, D., Fan, C., Wang, L., 2014. ACS Appl. Mater. Interfaces 6, 1152–1157.
Tang, B., Cao, L., Xu, K., Zhuo, L., Ge, J., Li, Q., Yu, L., 2008. Chem. – A Eur. J. 14, 3637–3644.
Thakar, R., Chen, Y., Snee, P.T., 2007. Nano Lett. 7, 3429–3432.
Traviesa-Alvarez, J.M., Sánchez-Barragán, I., Costa-Fernández, J.M., Pereiro, R., Sanz-Medel, A., 2007. Analyst 132, 218–223.
Wang, X., Lou, X., Wang, Y., Guo, Q., Fang, Z., Zhong, X., Mao, H., Jin, Q., Wu, L., Zhao, H., Zhao, J., 2010. Biosens. Bioelectron. 25, 1934–1940.
Wu, P., He, Y., Wang, H.-F., Yan, X.-P., 2010. Anal. Chem. 82, 1427–1433.
Wu, P., Miao, L.N., Wang, H.F., Shao, X.G., Yan, X.P., 2011. Angew. Chem. Int. Ed. 50, 8118–8121.
Wu, P., Zhang, J., Wang, S., Zhu, A., Hou, X., 2014a. Chem. – A Eur. J. 20, 952–956.
Wu, P., Zhao, T., Zhang, J., Wu, L., Hou, X., 2014b. Anal. Chem. 86, 10078–10083.
Xia, Z., Rao, J., 2009. Curr. Opin. Biotechnol. 20, 37–44.
Xu, Y., Piston, D.W., Johnson, C.H., 1999. Proc. Natl. Acad. Sci. USA 96, 151–156.
Yang, L.H., Ahn, D.J., Koo, E., 2016. Mater. Sci. Eng.: C 69, 625–630.
Ye, Y.-D., Xia, L., Xu, D.-D., Xing, X.-J., Pang, D.-W., Tang, H.-W., 2016. Biosens. Bioelectron. 85, 837–843.
Yildiz, I., Tomasulo, M., Raymo, F.M., 2006. Proc. Natl. Acad. Sci. USA 103, 11457–11460.
Zhang, C.-Y., Yeh, H.-C., Kuroki, M.T., Wang, T.-H., 2005. Nat. Mater. 4, 826–831.
Zhang, L., Cui P., Zhang B.,Gao F., 2013. Chemistry (Weinheim an der Bergstrasse, Germany) 19, pp. 9242–9250.
Zhao, D., Li, J., Yang, T., He, Z., 2014. Biosens. Bioelectron. 52, 29–35.
Zhou, D., Ying, L., Hong, X., Hall, E.A., Abell, C., Klenerman, D., 2008. Langmuir 24, 1659–1664.
Zhuang, J., Zhang, X., Wang, G., Li, D., Yang, W., Li, T., 2003. J. Mater. Chem. 13, 1853–1857.